# CMS Draft Analysis Note

*The content of this note is intended for CMS internal use and distribution only*

2018/11/16
Head Id: 481556
Archive Id: 481556
Archive Date: 2018/11/16
Archive Tag: trunk

# Searching for exclusively produced top quark pairs

B. Ribeiro Lopes[2], P. Silva[1], J. Hollar[2], and M. Gallinaro[2]

[1] CERN, Geneva, Switzerland
[2] LIP, Laboratório de Instrumentação e Física Experimental de Partículas, Lisbon, Portugal



## Abstract

A search for exclusive production of top quark pairs, where the outgoing unfragmented protons are detected about 210 m away from the centre of the CMS detector, is described. Proton-proton collision data at $\sqrt{s}$ =13 TeV collected in 2017 are used for the search. An upper limit is set on the production cross section.

# Contents

# 1 Introduction

This note reports on the search for exclusive top quark pairs, $pp \to p\mathrm{t\bar{t}}p$, where the $\mathrm{t\bar{t}}$ pair decays dileptonically. The process is represented by the Feynman diagrams in Fig. 1. If identified in the data, this production channel is characterized by the suppression of additional radiation in the central region. If the kinematics of the protons are measured, it offers the possibility of determining the $\mathrm{t\bar{t}}$ production threshold with a better resolution than the one that can be attained based on the inclusive production, through the reconstruction of the final states. The standard model (SM) prediction for the exclusive top pair production cross section is extremely small, $\mathcal{O}(1\ \mathrm{fb})$ for photo-production, and it lacks updated predictions [1]. However, if new physics is present, the small cross section can be significantly enhanced either in the production of $\mathrm{t\bar{t}}$ or in the production of similar final states containing at least two leptons [2–5].

In our analysis, the two leptons (electrons or muons) and the b-jets from the top quark decay are measured in the central CMS apparatus, while the two outgoing protons are measured in the Precision Proton Spectrometer (PPS). The latter is a near-beam magnetic spectrometer that uses the LHC magnets between the Interaction Point (IP) and detector stations at $\approx \pm 210$ m from the IP. Protons that have lost a small fraction of their momentum are bent out of the beam envelope so that their trajectories can be measured. The detectors that form PPS are called Roman Pots (RPs).

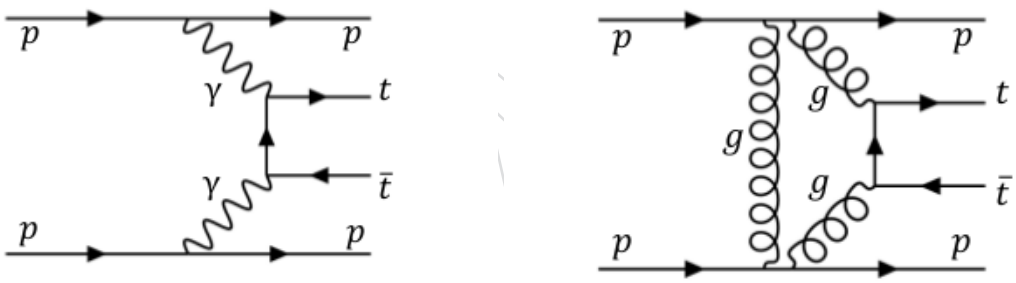


Figure 1: Exclusive $\mathrm{t\bar{t}}$ production diagrams, via $\gamma\gamma$ fusion (left) and $gg$ fusion (right).

# 2 Data and simulation samples

The analysis is performed using proton-proton collision data at $\sqrt{s} = 13$ TeV collected in 2017 by CMS. The SingleMuon and SingleElectron primary datasets (PDs) are used[1]. The events passing the triggers listed on Table 1 are considered in our analysis. The total integrated luminosity corresponds to 41.4 $\mathrm{fb}^{-1}$.

For the correlation between the central detector and the PPS, only data collected before Technical Stop 2 (TS2) are used. This is because both the detector efficiency and the PPS acceptance (due to new LHC optics) are different after-TS2 data and their measurement is still being finalized. In the PPS, RPs are identified followed by a 3-digit number, where the first digit is either 0 or 1 according to which arm the pot belongs to (0 for a positive z coordinate: z+, and 1 for negative z coordinate: z-), the second digit is the station number, and the third the RP number. RP numbered 003 and 103 contain silicon strip detectors, while those labeled 023 and

[1] These are chosen as the starting point for the analysis, but could be complemented in a future version with the DoubleElectron, DoubleMuon and MuEG datasets to maximize the efficiency for the dilepton final state.

Table 1: Triggers used in the selection of the events. Events where both the muon and one of the electron trigger fires are allowed only if they are found in the SingleMuon PD.

| Trigger name |
|---|
| HLT_Ele35_eta2p1_WPTight_Gsf_v |
| HLT_Ele28_eta2p1_WPTight_Gsf_HT150_v |
| HLT_Ele30_eta2p1_WPTight_Gsf_CentralPFJet35_EleCleaned_v |
| HLT_IsoMu27_v |

123 contain 3D pixel detectors. The scheme of the PPS detector and its arms is shown in Fig. 2. Only data from RPs 003, 023, 103 and 123 were used, since no alignment parameters exist for other RPs. Besides, only collisions with crossing angle of 120, 130 or 140 $\mu$rad are considered, because there are no dispersion values available for other crossing angles. The total integrated luminosity where combined CMS(central)-PPS data have been analysed with calibrated pixels is thus reduced to 18.7 fb$^{-1}$.


Figure 2: Scheme of the PPS detectors used in the analysis.

The official Monte Carlo production samples have been used for the background. The name of the samples and the cross section used to normalize them is summarized in Tab. 2.

Table 2: MC samples from the RunIIFall17MiniAOD-94X_mc2017_realistic_v10 production used in this analysis.

| Process | $\sigma$ [pb] | MC sample |
|---|---|---|
| $t\bar{t}$ | 832 | TTJets_TuneCP5_13TeV-amcatnloFXFX-pythia8 |
| ZZ$\rightarrow 2\ell 2\nu$ | 0.564 | ZZTo2L2Nu_13TeV_powheg_pythia8 |
| WZ | 47.13 | WZ_TuneCP5_13TeV-pythia8 |
| WW$\rightarrow 2\ell 2\nu$ | 12.178 | WWTo2L2Nu_NNPDF31_TuneCP5_13TeV-powheg-pythia8 |
| W+3jets | 942.3 | W3JetsToLNu_TuneCP5_13TeV-madgraphMLM-pythia8 |
| W+4jets | 524.2 | W4JetsToLNu_TuneCP5_13TeV-madgraphMLM-pythia8 |
| $\bar{t}$W | 35.85 | ST_tW_antitop_5f_NoFullyHadronicDecays_TuneCP5_13TeV-powheg-pythia8 |
| tW | 35.85 | ST_tW_top_5f_NoFullyHadronicDecays_TuneCP5_13TeV-powheg-pythia8 |
| DY (M>50 GeV) | 5765.4 | DYJetsToLL_M-50_TuneCP5_13TeV-amcatnloFXFX-pythia8 |

In addition, a signal $pp \rightarrow p\gamma p \rightarrow t\bar{t}pp$ sample has been produced privately using FPMC [6] as the matrix element generator and HERWIG++ [7] as the parton shower. This sample has been used to compute the acceptance and guide the final event selection.

# 3 Event selection

## 3.1 Central detector selection

Two charged leptons (electron or muon) with $M_{ll} > 20$ GeV are required. At least one of the leptons is required to have $p_T > 30$ GeV, while the second one is required to have $p_T > 15$ GeV. Both have to be reconstructed within $|\eta| < 2.5$. Depending on the flavour and invariant mass of the dilepton system, the events are classified in the following exclusive categories:

- same-flavour leptons ($ee$ or $\mu\mu$) with reconstructed $M_{ll}$ around the Z mass ($M_{ll} \in [76, 106]$ GeV): Z-control region;
- same-flavour leptons outside the Z peak region: SF region;
- opposite-flavour leptons ($e\mu$): OF region.

After categorizing the events, the following selection is applied:

- $\geq 1$ jet ($p_T > 20\,\text{GeV}$, $|\eta| < 4.7$ passing a loose pileup jet id criteria [8]);
- $\geq 1$ b-jet ($p_T > 30\,\text{GeV}$, $|\eta| < 2.5$ passing the deepCSV "medium" working point [9]);
- at least one lepton-b combination verifies $M_{lb} < 160\,\text{GeV}$.

In the last requirement $M_{lb}$ refers to the invariant mass of lepton-b jet system. All lepton-b jet combinations are used and the one with min $M_{lb}$ is considered for the final selection. The criterion stems from the fact that, by energy conservation, one expects at leading order (LO), that $M_{lb} < \sqrt{m_t^2 - m_W^2} \approx 160$ GeV for $m_t = 172.5\,\text{GeV}$ and $m_W = 80.4\,\text{GeV}$ [10]. Thus, by applying such requirement, we expect that higher $t\bar{t}$ purity is attained.

Figure 3 shows the distribution of the invariant mass of the dilepton system for the SF and OF categories. It can be observed that even after removing the Z peak region, the SF category is expected to be dominated by the Drell-Yan (DY) production. The excess in data for $m_{ll} < 50\,\text{GeV}$ is expected given the DY simulation does not include that region. For the OF category an overall excess is observed which may be attributed to missing simulated processes (to be checked).

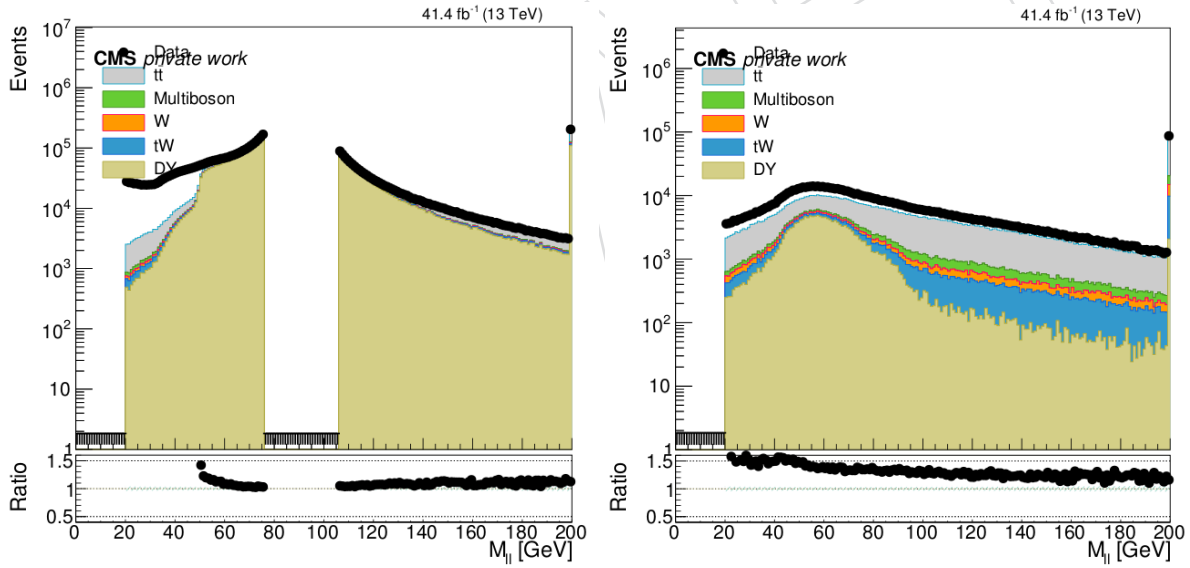


Figure 3: Control sample (central detector only): Distribution of the mass of the dilepton system after selecting 2 leptons, for same flavour leptons except events under the Z peak (left) and for opposite flavour leptons (right). The data is compared to the stacked predictions based on the simulation. The bottom panels show the ratio of the data to the total prediction.

Figure 4 shows the distribution of the b-tagging multiplicity. An excess is observed for events with low multiplicity in both the SF and OF categories. The excess disappears once the high purity region of $t\bar{t}$ is selected ($\geq 1$ b-tag).

Figure 5 shows the distribution of the $M_{lb}$ variable after the selection of at least 1 b-jet. An overall excess for the high $M_{lb}$ region is observed in both the SF and OF categories. This may

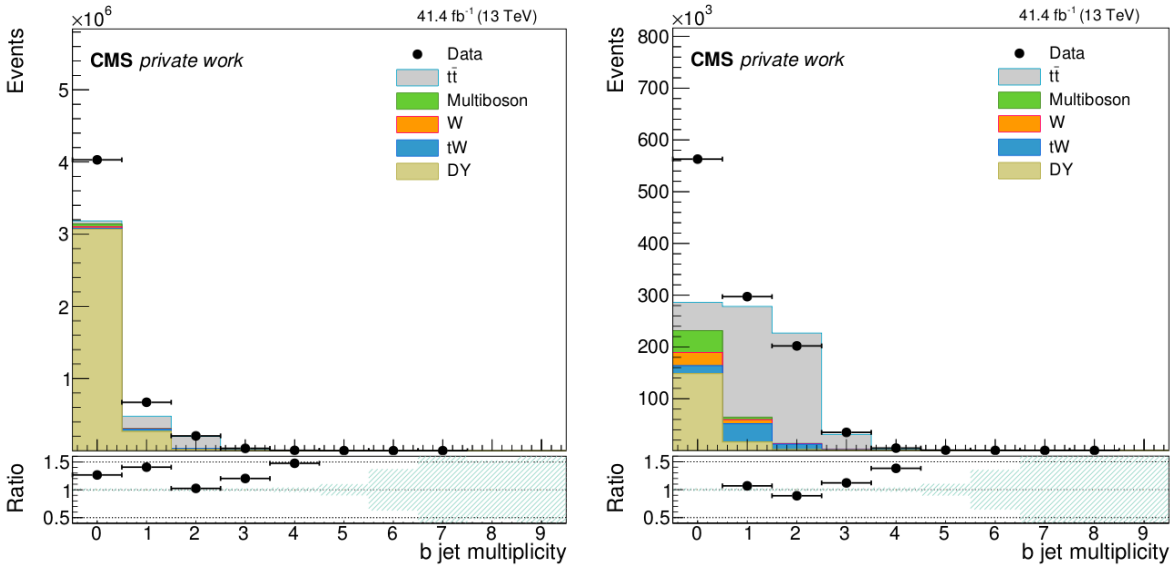


Figure 4: Control sample (central detector only): Number of b-tagged jets after requiring 2 leptons, for same flavour leptons except events under the Z peak (left) and for opposite flavour leptons (right).

be due to missing simulated samples (to be confirmed). In any case these events are removed from our analysis as the low $M_{lb}$ region is the one which is expected to be enriched in $t\bar{t}$ events.

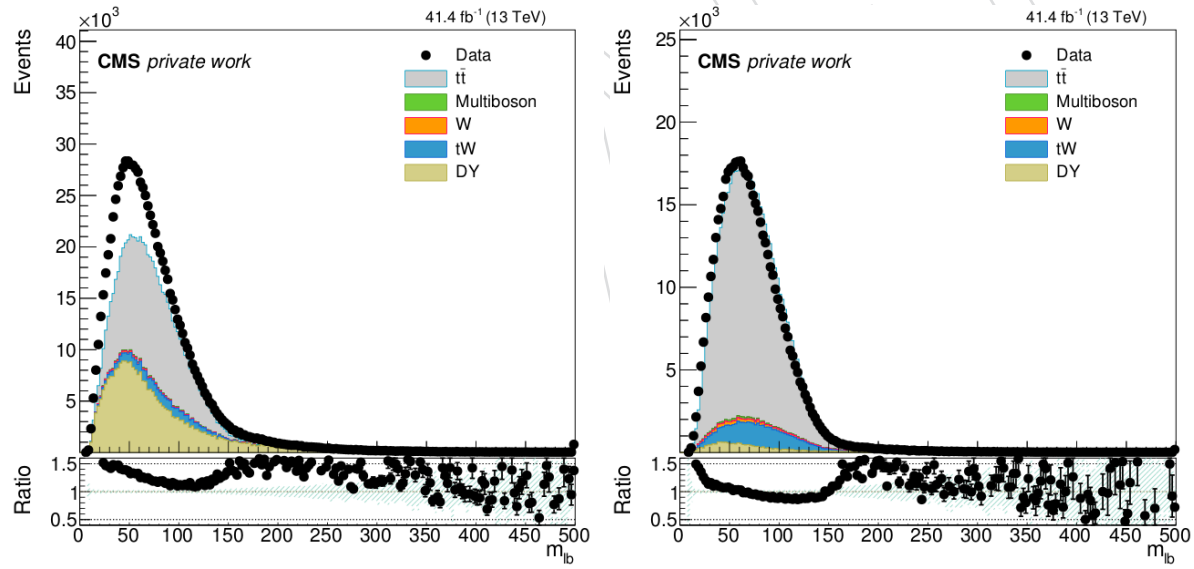


Figure 5: Control sample (central detector only): Mass of the lepton/b-jet system, after requiring 2 leptons, 1 jet and 1 b-jet, for same flavour leptons except events under the Z peak (left) and for opposite flavour leptons (right).

We have compared the signal and the inclusive $t\bar{t}$ sample with respect to specific variables reconstructed in the central detector. The variables were chosen to be sensitive to the additional hadronic activity which is expected to be suppressed in the case the production is exclusive and via electroweak vertices. The variables chosen are:

- $H_T = \sum_{j=1}^{N_j} |\vec{p}_{\mathrm{T,j}}|$, the scalar sum of the transverse momentum of all jets except the b-jets;
- Hadronic recoil $h = |\vec{p}_T^{\,miss} + \vec{p}_T(\ell_1) + \vec{p}_T(\ell_2) + \sum_{j=1}^{N_b} \vec{p}_T(j)|$, obtained from the sum

of the missing transverse energy with the two charged leptons and up to two b-jets. In the analysis we make use of the so-called puppiMET estimator for $\vec{p}_T^{miss}$ [11].

In the simulations we observe that signal $t\bar{t}$ has a considerably small fraction of events which have extra activity, that is most of the events have $H_T$=0 given there are no extra jets in the event. Conversely signal $t\bar{t}$ events tend to have lower $h$ when compared to inclusive $t\bar{t}$ productions. Figure 6 shows the distribution of these variables in data and simulation. A slight trend is observed with respect to the predictions, but no systematic uncertainties (e.g. related to pileup, and the jet energy scale) have been used at this point.

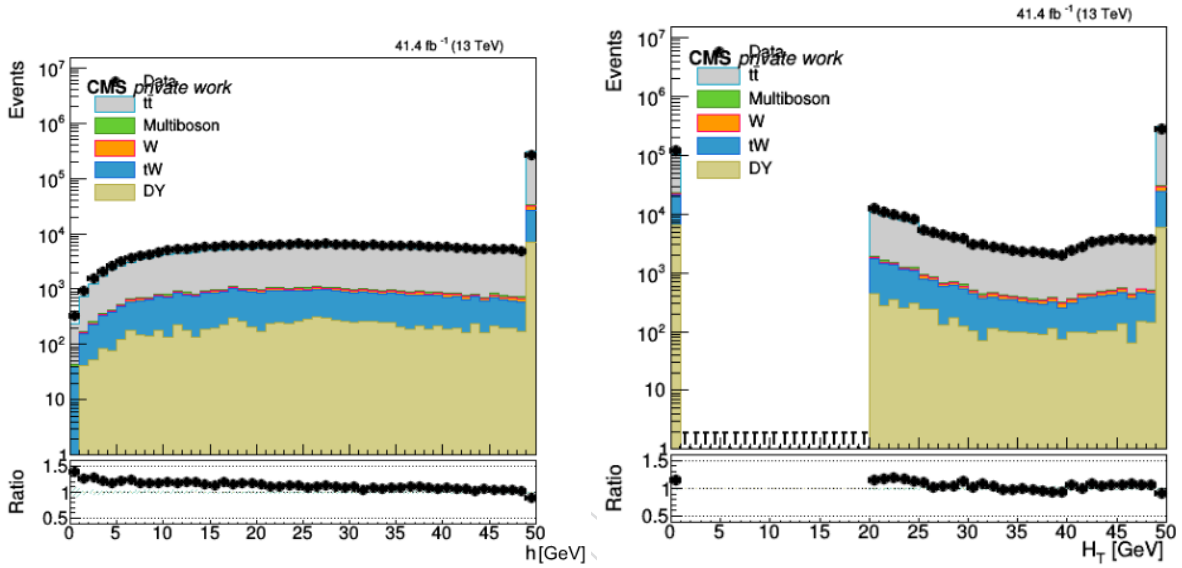


Figure 6: Control sample (central detector only): Hadronic activity distributions obtained after requiring 2 leptons, 1 jet, 1 b-jet, $M_{lb}$ <160 GeV and opposite flavour leptons. The hadronic recoil $h$ (left) and $H_T$ (right) are shown.

A comparison between distributions in signal and inclusive $t\bar{t}$ was furthermore performed for the two important hadronic activity variables. Figure 7 depicts that the observed difference is significant between the two $t\bar{t}$ production mechanisms. This information can be used to purify the event selection. In this analysis we shall require that $H_T = 0$ GeV in the signal region.

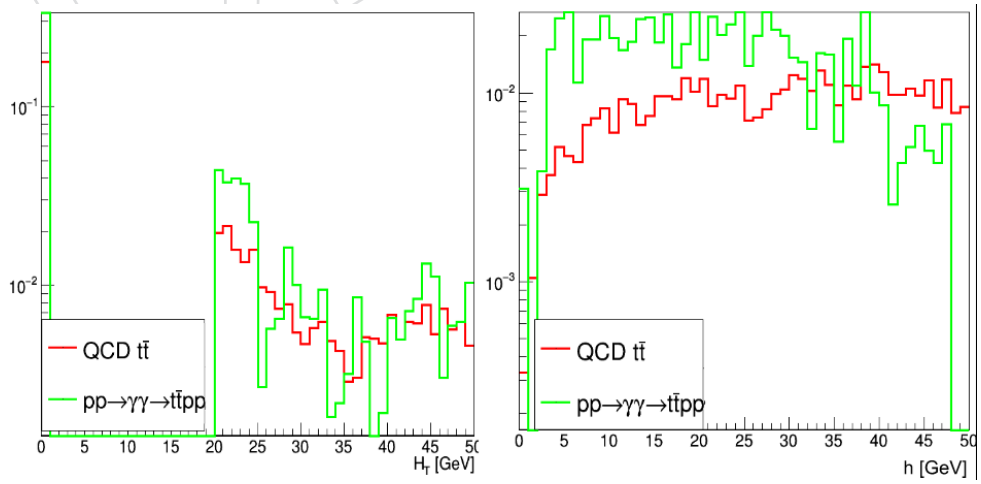


Figure 7: Control sample (central detector only): Normalized distribution of $H_T$ (left) and $h$ for signal and inclusive $t\bar{t}$. The distributions have been normalized to unity.

## 3.2 PPS detector selection

For the final selection we use data from the pixel detectors. The choice for the pixels is made given that they are able to reconstruct more than one track per event, so in case of pileup the signal is not lost due to inefficency of the reconstruction. For events each track reconstructed in the pixel detector one is able to reconstruct the fractional momentum loss ($\xi$) of the proton. The $\xi$ distribution for each pixel can be seen in figure 8, for a fraction of the data set.

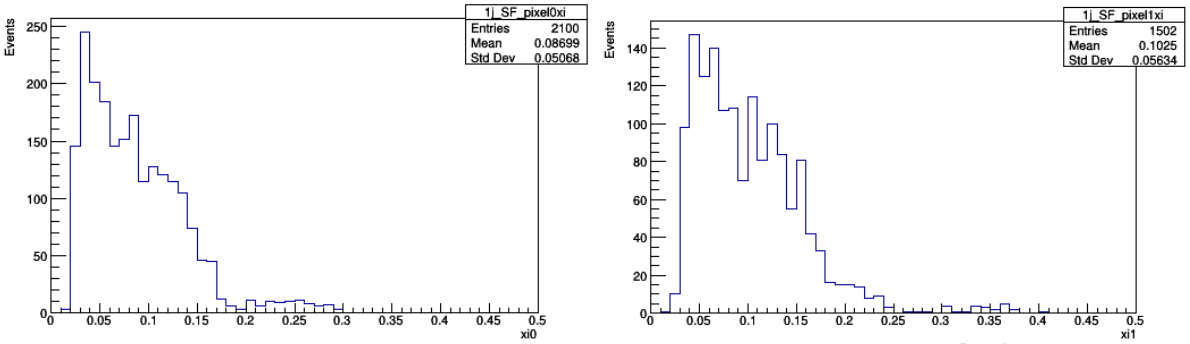


Figure 8: Distribution of the fractional momentum loss ($\xi$) of the protons detected in the pixels, for RP023 (left) and RP123 (right) (for a fraction of the data set).

From the value of $\xi$, one reconstructs the mass and rapidity of the $t\bar{t}$ in the central system, using the following equations:

$$M_{RP} = \sqrt{s\xi_0\xi_1} \tag{1}$$

$$y_{RP} = \frac{1}{2}\ln\left(\frac{\xi_0}{\xi_1}\right) , \tag{2}$$

where the subscripts 0 and 1 refer to the arm number.

Due to pileup (the average vertex multiplicity in the 2017 data is $\sim$30), there is often more than one track per event in each pixel detector. Thus there is the need to reconstruct the mass and rapidity for every combination of tracks. The plots in figure 9 show the obtained distributions in mass and rapidity.

In this analysis we selected events in the $M_{RP} \in [300, 600]$GeV range, which is chosen to be compatible with the bulk of the production threshold of exclusive $t\bar{t}$. The events are categorized depending on whether or not there is a combination of tracks that leads to a reconstructed $t\bar{t}$ mass in this range.

## 3.3 Matching the central and the forward kinematics

A further improvement in the S/B ratio may be achieved by matching the kinematics of the events reconstructed in the central and in the PPS detectors. We apply the algorithm described in [12] to reconstruct the kinematics of the central system for the selected events. The algorithm is applied to the events which pass the full selection described before. Given the ambiguity in the pairing of the leptons and the b jets and in the kinematics of the two outgoing neutrinos, up to 8 solutions can be found per event. We have chosen the solution which yields the lowest $M_{t\bar{t}}$. After this choice, the mass and rapidity computed from the forward tracks can then be compared with the ones reconstructed using the central system. The correlation between the

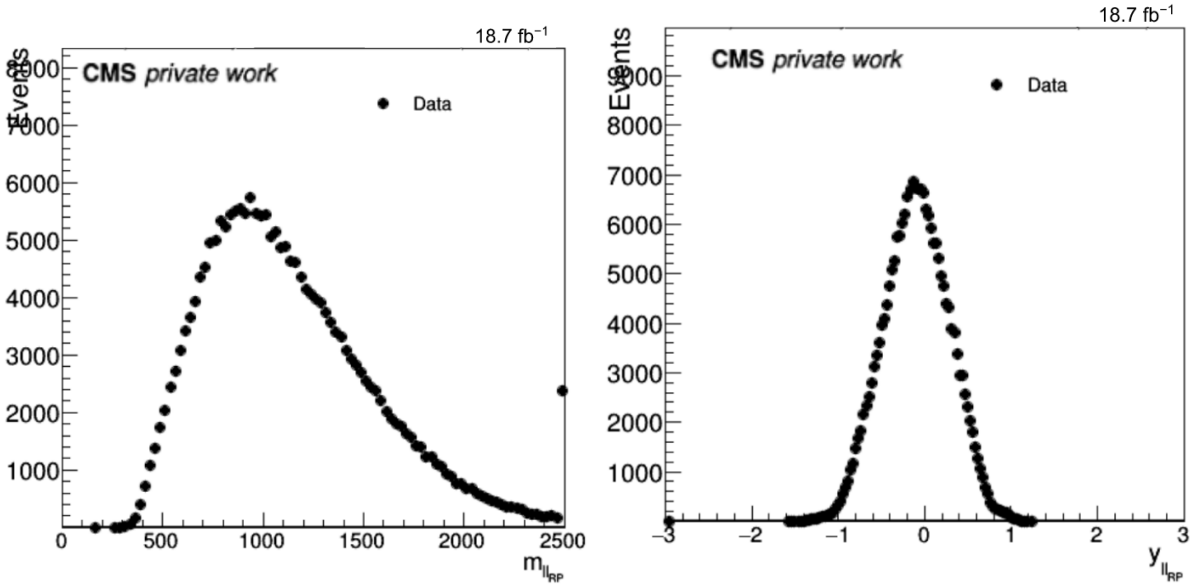


Figure 9: Distribution of the reconstructed mass (left) and rapidity (right) of the dilepton system in the RPs, when requiring 2 leptons of opposite flavour.

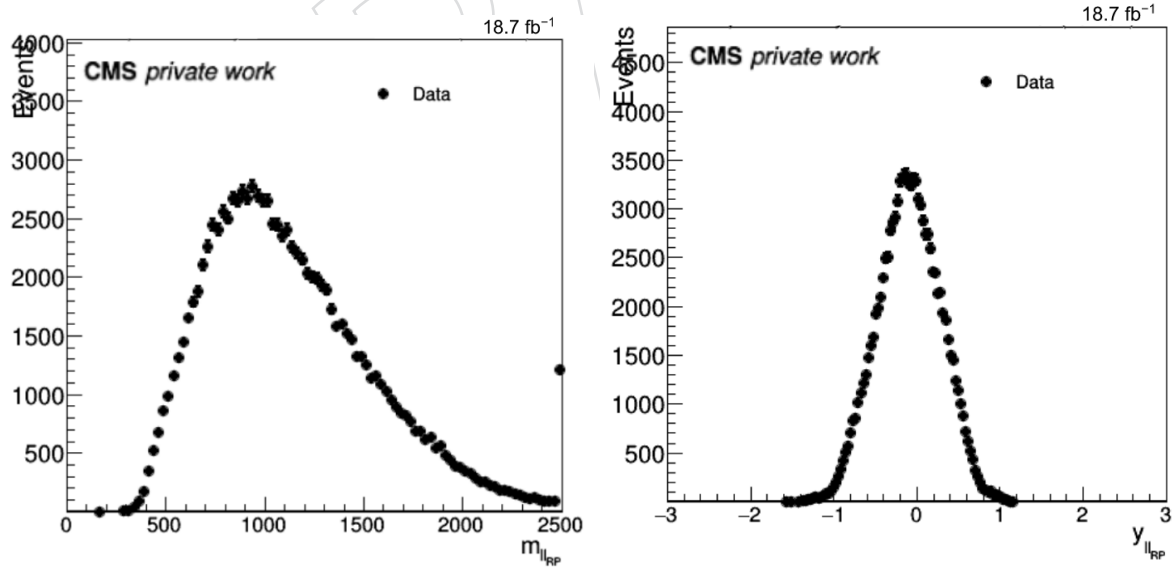


Figure 10: Distribution of the reconstructed mass (left) and rapidity (right) of the dilepton system in the RPs, when requiring 2 leptons of opposite flavour, 1 jet, 1 b-jet, low mass of the lepton/b-jet system.

two can be found in Fig. 11. At this point no correlation is however observed, i.e. the selected region is still largely dominated by inclusive $t\bar{t}$ events and pileup combinatorics in the roman pots. Fig. 12 shows the same correlation, but for simulated $t\bar{t}$ events. We can see that for rapidity the reconstruction performs quite well, but that is not the case for the mass.

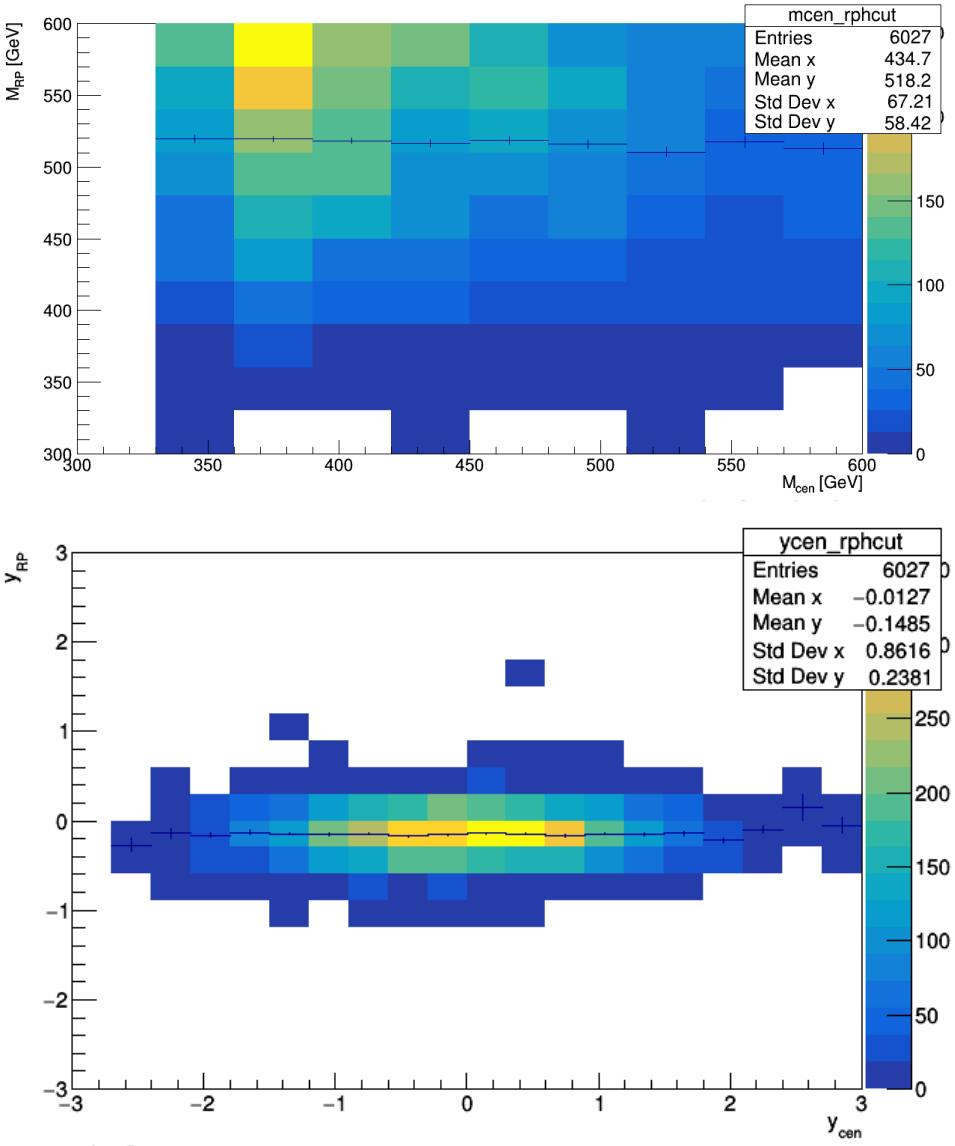


Figure 11: 2D plots of the mass (top) and rapidity (bottom) of the dilepton system reconstructed using the mentioned algorithm for the selected events ($m_{cen}$, $y_{cen}$) versus the mass and rapidity reconstructed from the RP tracks ($m_{RP}$, $y_{RP}$). The profile of each distribution is overlaid.

# 4 Background determination

The most important background is due to non-exclusive $t\bar{t}$ events combined with random pileup protons that are detected in PPS. This background is determined with a data-driven method. For this purpose, a combinatorial analysis is performed, where one takes the number of tracks per event and the $\xi$ distributions in each pixel as observed at pre-selection level where possible contribution from signal is negligible. For each event, one generates a random number

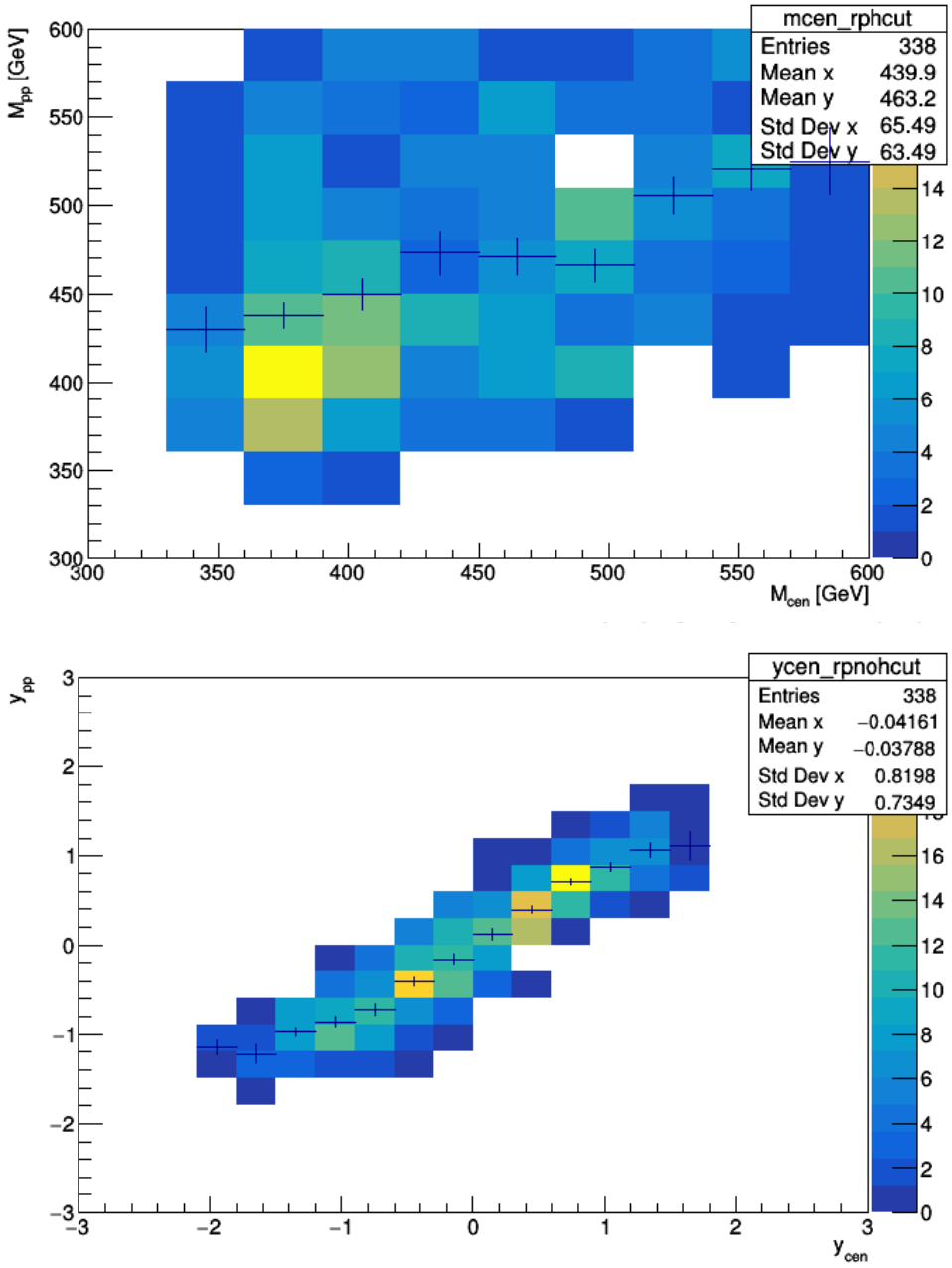


Figure 12: 2D plots of the mass (top) and rapidity (bottom) of the dilepton system reconstructed using the mentioned algorithm for simulated $t\bar{t}$ events ($m_{cen}$, $y_{cen}$) versus the mass and rapidity of the two protons in the simulation ($m_{pp}$, $y_{pp}$). The profile of each distribution is overlaid.

of tracks and a random $\xi$ value for each of these tracks on each side of the PPS detector. This allows to reconstruct random pairs of tracks from where the mass and rapidity of the candidate combinatorial pp pairs can be computed. If one of these combinatorial pairs is found to have a mass within the $[300, 600]$ GeV range, the event is counted. Finally, the number of events selected is divided by the initial number of events in the sample and the fraction of random coincidences is measured. We estimate the probability of random coincidences in this mass range to be ≈3.34% with negligible statistical uncertainty. The result is similar for the SF, OF, and Z peak categories.

This fake rate can be applied to all non-exclusive backgrounds and thus used to project the yields of non-exclusive $t\bar{t}$, tW, DY and dibosons in the signal region. There may be, however, other subleading backgrounds that are not being considered, such as semi-exclusive $t\bar{t}$ events (where only one proton stays intact) with 1 pileup proton.

In addition, the events which do not pass the combinatorial pair selection (or the pair selection in data) are counted in separate categories which are used to normalize from data the initial estimates for $t\bar{t}$ and DY. The latter is normalized from SF events under the Z peak.

# 5 Determination of Roman Pot acceptance

In order to estimate the acceptance of the Roman Pots for the the $pp \to pt\bar{t}p$ signal, the sample generated with FPMC+Herwig has been used. A 2D distribution comparing the mass and the rapidity of the simulated $t\bar{t}$ system is calculated, requiring 2 leptons in the final state. Then, a cut is applied by selecting only events that fall within the RP acceptance expected range for $\xi$, i.e. $0.02 < \xi < 0.2$. The plots before and after the cut are shown in figure 13. From these plots, one simply divides the number of surviving events by the initial number of all simulated events. The acceptance of the Roman Pots is measured to be 1.01%. This estimate is preliminary and could be further improved by considering that the RPs have an asymmetric acceptance between the two arms (see for example the $\xi$ distributions in figure 8) and by taking the minimum and maximum values from the $\xi$ distributions for each arm, instead of using a fixed expected range. However, the difference is not expected to be very significant.

| selection step | Surviving events | |
|---|---|---|
| Initial number of simulated events | 35920 | 100% |
| Events with 2 leptons | 1330 | 3.70% |
| Events in RP acceptance | 361 | 1.01% |

Table 3: RP acceptance: number of events surviving the selection cuts and their corresponding fractions.

# 6 Determination of $\sigma(pp \to pp2\ell1b)$ through a statistical analysis

The final event yields, including the extrapolation of the backgrounds in the signal region using the fake rate method described in Sec. 4 are shown in Tab. 4. The 5 different categories share in common the selection of:

- $\geq 2$ leptons with $M_{ll}$ >20 GeV;
- $\geq 1$ b-jet;
- $M_{lb} < 160$ GeV.

The specific requirements of the final event categories are the following:

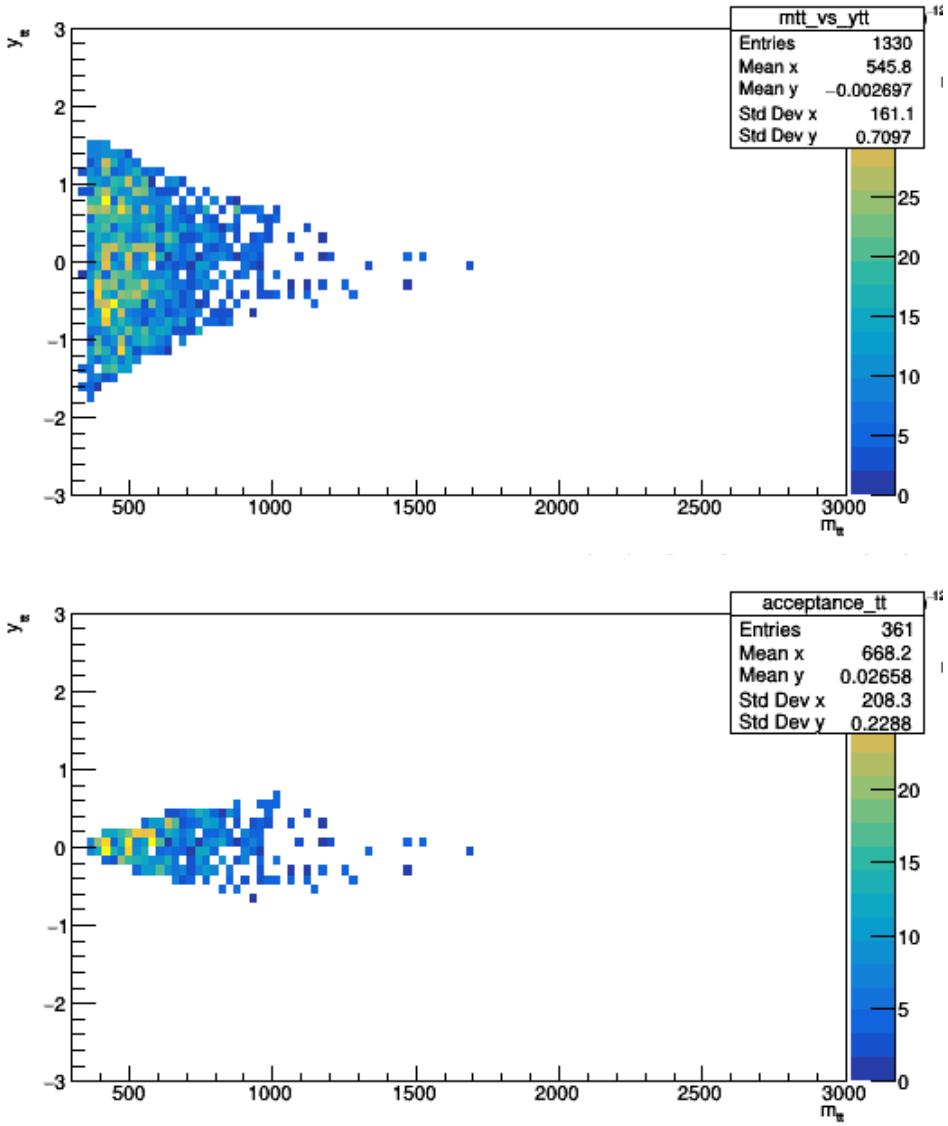


Figure 13: 2D distributions of the mass ($m_{RP}$) versus rapidity ($y_{RP}$) of the $t\bar{t}$ system in the signal sample, just requiring 2 leptons (left) and after requiring the tracks to be within the RP acceptance ($0.02 < \xi < 0.2$) (right).

**SR_OF** - $e\mu$ events with $M_{RP} \in [300, 600]$ GeV and $H_T = 0$ GeV;

**SR_SF** - similar to SR_OF for same flavour events outside the Z peak;

$\mathrm{t\bar{t}}$ **CR_OF** - $e\mu$ events failing the $M_{RP} \in [300, 600]$ GeV cut;

$\mathrm{t\bar{t}}$ **CR_SF** - similar to $\mathrm{t\bar{t}}$ CR_OF for same flavour events outside the Z peak;

**dyCR** - similar to $\mathrm{t\bar{t}}$ CR_SF but for same flavour events inside the Z peak.

In the following, we perform a combined fit of the event yields observed in each category.

| Process | SR_SF | SR_OF |
|---|---|---|
| inclusive $\mathrm{t\bar{t}}$ | 1172 | 1460 |
| DY | 1742 | 97 |
| others | 30 | 34 |
| total | 2944 | 1591 |
| data | 2538 | 1130 |

Table 4: Yields in the signal region for different background contributions and for those observed in data.

| Process | $\mathrm{t\bar{t}}$ CR_SF | $\mathrm{t\bar{t}}$ CR_OF | dyCR |
|---|---|---|---|
| inclusive $\mathrm{t\bar{t}}$ | **415937** | **519492** | 114783 |
| DY | 271583 | 17395 | **2863390** |
| others | 9962 | 12180 | 11756 |
| total | 697483 | 549068 | 2989929 |
| data | 903621 | 550805 | 3759454 |

Table 5: Yields in the control regions for different background contributions and those observed in data.

## 6.1 Method employed in the statistical analysis

The number of events observed in the signal and control regions can be analyzed to set limits on the production cross section of $pp \to pp2\ell1b$. In order to do it we parametrize the total number of events expected in a single category as follows:

$$N_{\mathrm{exp}} = N_{\mathrm{exp}}(pp \to pp2\ell1b) + f \cdot \left[N_{\mathrm{exp}}(\mathrm{t\bar{t}}) + N_{\mathrm{exp}}(\mathrm{tW}) + N_{\mathrm{exp}}(\mathrm{DY}) + N_{\mathrm{exp}}(\mathrm{others})\right] \quad (3)$$

where $f$ is the probability that a non-exclusive event passes the selection of the RPs due to combinatorial tracks. In Eq. 3 we assume that there is no additional exclusive process which may contribute in the selected regions. The CRs for $\mathrm{t\bar{t}}$ and DY are used to normalized the initial expectations based on simulation. We thus employ $\mu_{\mathrm{t\bar{t}}}$ ($\mu_{\mathrm{DY}}$) as scaling factors of the initial expectations for $\mathrm{t\bar{t}}$ (DY), i.e.:

$$N_{\mathrm{exp}}(b) = \mu_b \cdot N^{\mathrm{MC}}_{\mathrm{exp}}(b) \quad (4)$$

where b=$\mathrm{t\bar{t}}$, DY and $N^{\mathrm{MC}}_{\mathrm{exp}}(b)$ is the expectation from simulation which includes the theory cross section, the integrated luminosity, and the corrections for the simulated efficiency with data-MC scale factors. Other processes in Eq. 3 will float constrained according to the estimated uncertainty. The expectations for the signal are written as a product of the following factors:

$$N_{\text{exp,c}}(pp \to pp2\ell1b) = A \cdot L \cdot \varepsilon_{\text{c}} \cdot \sigma(pp \to pp2\ell1b) \tag{5}$$

where c=SF, OF is the event category, $A$ is the acceptance at generator level for the selection of two leptons and an invariant mass of the outgoing protons in the acceptance of the PPS detector, $L$ is the total integrated luminosity, $\varepsilon_{\text{c}}$ is the efficiency of the selection and $\sigma_p p \to pp2\ell1b$ is the cross section. Given that the selection criteria differ slightly in the SF and OF categories, in Eq. 5, the efficiency factors are computed separately for each category. With these definitions in hand we can maximize the following likelihood as function of $\sigma_p p \to pp2\ell1b$

$$\mathcal{L} = \prod_{k=1}^{N} \mathcal{P}_{\text{oisson}}(N_{\text{obs}}|N_{\text{exp}}) \cdot \prod_{m=1}^{M} f(\theta_k) \tag{6}$$

where the first product runs over the $N$ categories in which events are counted, and the second product runs over $M$ nuisance parameters which encode the relative uncertainty of the parameters employed to parametrized the expectations $N_{\text{exp}}$. The PDF $f(\theta_k)$ is taken as a log-normal function. The implementation of Eqs 3- 6 is made in RooStats, using the Higgs Combination Tool.

## 6.2 Summary of the inputs to the statistical analysis

Table 6 summarizes the values used for the acceptance, efficiency, and the final product of those with the integrated luminosity in which the PPS data was analysed. The summary of the systematic uncertainties considered in the fit is in Tab. 7.

| | SF | OF |
|---|---|---|
| Signal acceptance | 0.0101 | |
| Selection efficiency (low $M_{lb}$) | 0.345 | 0.428 |
| N (luminosity * acc. * eff.) | 65.055 | 80.697 |

Table 6: Summary table of some inputs to the statistical analysis. Signal acceptance, the selection efficiency in the signal region (low $M_{lb}$), number of expected events, Numbers are shown for same flavour and opposite flavour categories.

| Uncertainty | Value | Affects |
|---|---|---|
| Luminosity | 2.7% | all processes |
| $\sigma_{\text{inclusive } \bar{\text{t}}\text{t}}$ | 5.1% | inclusive $\bar{\text{t}}\text{t}$ (SR and CR) |
| $\sigma_{\text{others}}$ | 30% | others |
| DY uncertainty | 30% | Drell-Yan |
| Fake rate | 5% | all processes except signal |
| Lepton selection efficiency | 3% | all processes |

Table 7: Systematic uncertainties used in the analysis.

## 6.3 Results

Using the Higgs Combination Tool with the inputs in section 6.2, one can obtain the likelihood plots shown in figure 14. It is then possible to get an asymptotic upper limit on the exclusive $\bar{\text{t}}\text{t}$ cross section: $\sigma < 900^{+360}_{-253}$ fb (68% confidence level), or $900^{+415}_{-788}$ fb (95% confidence level).

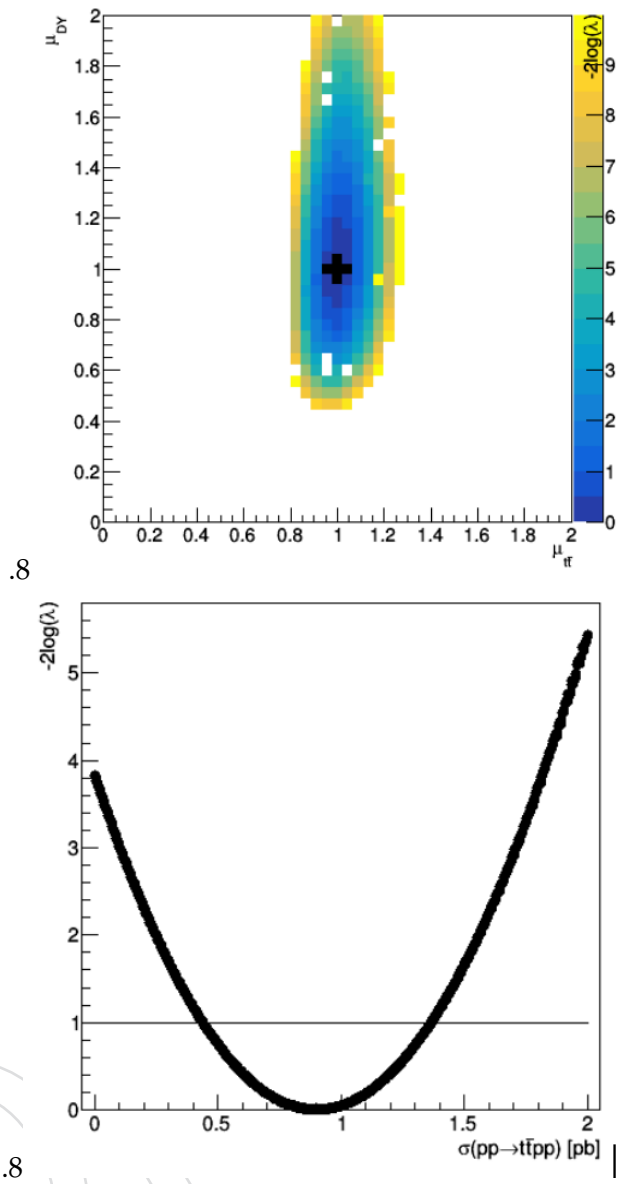


Figure 14: (a) Contour of the likelihood for the scale factor for inclusive $t\bar{t}$ and DY processes which are fit using the dedicated control regions. The point marks the fitted values. (b) Likelihood scan results for the signal at expectation level for a $\sigma = 900$ fb scenario. The line intersects the likelihood at the boundaries of the 68% CI.

# 7 Conclusions

We analyse 2017 data searching for exclusive $t\bar{t}$ production in the dilepton final state. An inclusive selection for two leptons and at least one b jet is studied and the background estimated. Signal discrimination variables are studied based on a dedicated simulation of $pp \to \gamma\gamma pp \to pt\bar{t}p$. The estimated upper limit on the production cross section of exclusive $t\bar{t}$ production is 900 fb.

# References


[1] J. de Favereau de Jeneret et al., "High energy photon interactions at the LHC", arXiv:0908.2020.

[2] P. J. Bussey, T. D. Coughlin, J. R. Forshaw, and A. D. Pilkington, "Central exclusive production of longlived gluinos at the LHC", *JHEP* **11** (2006) 027, doi:10.1088/1126-6708/2006/11/027, arXiv:hep-ph/0607264.

[3] S. Heinemeyer et al., "Central Exclusive Production of BSM Higgs bosons at the LHC", in *Proceedings, 38th International Symposium on Multiparticle Dynamics (ISMD 2008): Hamburg, Germany, September 15-20, 2008*, pp. 338–343. 2009. arXiv:0811.4571. doi:10.3204/DESY-PROC-2009-01/60.

[4] S. Taheri Monfared and S. Fayazbakhsh, "Probing Anomalous Top Quark Couplings in Diffractive Events at the LHC", *Acta Phys. Polon. Supp.* **7** (2014), no. 3, 579, doi:10.5506/APhysPolBSupp.7.579.

[5] K. Piotrzkowski and N. Schul, "Two-photon exclusive production of supersymmetric pairs at the LHC", *AIP Conf. Proc.* **1200** (2010) 434–437, doi:10.1063/1.3327609, arXiv:0910.0202.

[6] M. Boonekamp et al., "FPMC: A Generator for forward physics", arXiv:1102.2531.

[7] M. Bahr et al., "Herwig++ Physics and Manual", *Eur. Phys. J. C* **58** (2008) 639–707, doi:10.1140/epjc/s10052-008-0798-9, arXiv:0803.0883.

[8] JME group Collaboration, "Jet identification in high pile-up environment ", twiki, 2017.

[9] CMS Collaboration, "Identification of heavy-flavour jets with the CMS detector in pp collisions at 13 TeV", *JINST* **13** (2018), no. 05, P05011, doi:10.1088/1748-0221/13/05/P05011, arXiv:1712.07158.

[10] Particle Data Group Collaboration, "Review of Particle Physics", *Phys. Rev. D* **98** (2018), no. 3, 030001, doi:10.1103/PhysRevD.98.030001.

[11] CMS Collaboration, "Performance of missing transverse momentum in pp collisions at $\sqrt{s} = 13$ TeV using the CMS detector", Technical Report CMS-PAS-JME-17-001, CERN, Geneva, 2018.

[12] B. A. Betchart, R. Demina, and A. Harel, "Analytic solutions for neutrino momenta in decay of top quarks", doi:10.1016/j.nima.2013.10.039, arXiv:arXiv:1305.1878.